 CMES, vol.7, no.3, pp.321-338, 2005

Two-Dimensional BEM Thermoelastic Analysis of Anisotropic Media with Concentrated Heat Sources

Y.C. Shiah[1], T.L. Guao[1] and C.L. Tan[2]

Abstract: It is well known in elastic stress analysis using the boundary element method (BEM) that an additional volume integral appears in the basic form of the boundary integral equation if thermal effects are considered. In order to restore this general numerical tool as a truly boundary solution technique, it is perhaps most desirable to transform this volume integral exactly into boundary ones. For general 2D anisotropic thermoelastostatics without heat sources, this was only achieved very recently. The presence of concentrated heat sources in the domain, however, leads to singularities at these points that pose additional difficulties in the volume-to-surface integral transformation. In this paper, the steps to overcome these difficulties are described and the integral transformation is successfully achieved for BEM implementation in a mapped plane. Three numerical examples are presented to demonstrate the veracity of the analytical and numerical formulations.

keyword: Boundary element method, anisotropic thermoelasticity, concentrated heat sources

1 Introduction

The elasticity problem of determining the stress field of an anisotropic medium with concentrated (point) heat sources or heat sinks has many important applications in engineering. Examples include point-soldering treatments of electronic circuit boards, internal cooling of single crystal alloys, and heat source channels in bed-rock foundations. Analytical solutions have been obtained for a few specific problems (see e.g. Clements (1973); Rahman (2003); Oin (1999); Sherief and Magahed (1999)), but recourse to numerical methods is often necessary for most practical problems. Among the most popular of these methods for general engineering analysis are the finite difference method, the finite element method (FEM), and the boundary element method (BEM). When modeling these problems which involve a discrete distribution of heat sources using the first two approaches, it is often necessary to employ very refined grids or meshes in the vicinity of the concentrated heat sources to ensure satisfactory accuracy, thereby giving rise to relatively complex internal mesh designs.

The BEM has been recognized as an efficient computational alternative due to its distinctive feature that only boundary discretisation of the solution domain is required. However, in its formulation for elastostatics, thermal effects manifest themselves as an additional volume integral in the boundary integral equation (BIE). Any attempt to directly integrate the volume integral will involve domain discretisation that destroys the notion of it being a truly boundary solution technique. Several schemes have been proposed over the years to obviate this. They include the Monte Carlo method, Camp and Gipson (1992)), particular integral approach, Deb and Banerjee (1990), the dual reciprocity method, Nardini and Brebbia (1982), the multiple reciprocity method, Nowak and Brebbia (1989), and the exact transformation method (ETM), Rizzo and Shippy (1977). A review of these schemes has also been provided recently by Cheng, *et al* (2001). Other more recent related contributions include those by Ochiai and Sladek (2004), Sladek, Sladek and Atluri (2004) and Rashed (2004). Among these, the ETM, developed originally for isotropic thermoelasticity, is fundamentally most appealing because it restores the BEM analysis as a purely boundary solution technique without incurring simplifying approximations. It is thus directly applicable to problems with re-entrant corners and cracks.

Although the ETM is now well established to treat

[1] Department of Aerospace and Systems Engineering, Feng Chia University, Taiwan, R.O.C.
[2] Corresponding Author, Dept. of Mechanical & Aerospace Engineering, Carleton University, Ottawa, Canada K1S 5B6
Tel. 1-613-520 2600 ext. 5699, Fax. 1-613-520 5715, Email: ctan@mae.carleton.ca

the volume integral associated with thermal effects in isotropic elasticity, a similar transformation for anisotropic elasticity was only achieved quite recently, when Shiah and Tan (1999a) employed a domain mapping technique, Shiah and Tan (1998), to facilitate the process. By removing the singularity at the source point for interior stress calculations, Shiah and Tan (1999b) also derived the Somigliana's identity for the stresses and strains at interior points resulting from general thermal effects. These authors further demonstrated the direct applicability of the ETM to crack problems in 2D anisotropic thermoelasticity in Shiah and Tan (2000).

In this paper, the work for treating the general anisotropic thermoelasticity problem is extended to consider a discrete distribution of concentrated heat sources present in the domain. The problem under consideration, although common and important in engineering, remains relatively unexplored in BEM. Due to the presence of concentrated heat sources, all temperature-related values, including the temperature itself and its spatial gradients, are singular at the heat source points. To ensure the analyticity of the integrand of the volume integral arising from the thermal effects for the volume-to-surface integral transformation, these singularities must be mathematically removed from the domain. Starting from the treatment of the associated anisotropic thermal field, the steps to solve the thermoelasticity problem will next be presented next. Some numerical examples are then provided to illustrate the validity and applicability of the proposed scheme.

2 2D Thermal Field with Concentrated Heat Sources

As is usual in treating a thermoelasticity problem, the temperature field is first obtained. It will be clear in later derivations for the transformed BIE, consideration of the associated thermal field is not only a precursor but also an integral part in the treatment of the BIE in thermoelasticity. Thus it is worthwhile examining first, the treatment of the associated thermal field. For steady state heat conduction in an anisotropic medium involving a discrete distribution of n internal concentrated heat sources, the governing partial differential equation may be expressed as

$$K_{ij}\Theta_{,ij} = -\sum_{m=1}^{n} S_m \delta_m(\vec{p}-\vec{M}_m) \quad , \quad (i,j=1,2) \tag{1}$$

where Θ represents the temperature change and , the conductivity coefficients. In Eq. (1), the right-hand-side represents the sum of the effects of the n concentrated heat sources with intensity S_m at the $m-$th point M_m, and δ_m denotes the Dirac delta function at point $\boldsymbol{p}$. From thermodynamic considerations and the Onsagar's reciprocity relation, the thermal conductivity coefficients must, in two-dimensions, satisfy the following

$$K_{11}>0 \ , \ K_{22}>0 \ , \ K_{12}=K_{21}, \quad K_{11}K_{22}-K_{12}^2>0 \tag{2}$$

A BEM approach to treat the anisotropic heat conduction problem is to employ the fundamental solution for the differential operator of Eq. (1) directly together with Green's identities, as adopted by Mera, *et al* (2001) recently. A more common approach, however, is to reduce Eq. (1) into its canonical form by changing the spatial coordinates so that the generally anisotropic problem becomes mathematically an orthotropic one. To this end, the principal axes (ζ_1, ζ_2) are first determined by rotating the original Cartesian axes such that the cross-derivative terms disappear. In the rotated Cartesian coordinate system, the governing equation in the absence of heat sources becomes

$$K_1^*\frac{\partial^2\Theta}{\partial\zeta_1^2}+K_2^*\frac{\partial^2\Theta}{\partial\zeta_2^2}=0 \tag{3}$$

where K_i^* represents the conductivity coefficients in the i-direction of the principal axis. This approach has been used in the finite element method, Segerlind (1984), the finite difference method, Li (1983), and also the BEM, Bruch and Lejeune (1989). The procedure to further reduce Eq. (3) into the canonical form of the standard Laplace's equation by scaling the principal coordinates has also been discussed in, e.g., Barnerjee and Butterfield (1981).

A variation of the above-mentioned approach is to employ a linear coordinate transformation such that Θ in the transformed domain is governed by the standard Laplace equation, Shiah and Tan (1998). For two-dimensional cases, the linear transformation between both coordinate systems may be expressed in general matrix form as

$$\begin{aligned} [\hat{x}_{\underline{1}}\ \hat{x}_{\underline{2}}]^T &= [F(K_{ij})]\,[x_1\ x_2]^T \\ [x_1\ x_2]^T &= [F^{-1}(K_{ij})]\,[\hat{x}_{\underline{1}}\ \hat{x}_{\underline{2}}]^T \end{aligned} \tag{4}$$

where $\mathbf{F}=[F(K_{ij})]$ and $\mathbf{F}^{-1}=[F^{-1}(K_{ij})]$ are the transformation and the inverse transformation matrices, respectively, in terms of the invariant coefficients. They

have component elements $[F_{mn}(K_{ij})]$ and $[F^{-1}_{mn}(K_{ij})]$, respectively, given below, Shiah and Tan (1998).

$$\mathbf{F} = \begin{pmatrix} \sqrt{\Delta}/K_{11} & 0 \\ -K_{12}/K_{11} & 1 \end{pmatrix}, \quad \mathbf{F^{-1}} = \begin{pmatrix} K_{11}/\sqrt{\Delta} & 0 \\ K_{12}/\sqrt{\Delta} & 1 \end{pmatrix}$$
$$\Delta = K_{11}K_{22} - K_{12}^2 \tag{5}$$

This linear transformation has the distinct advantage of allowing the analysis to be carried out using any standard BEM code for isotropic potential theory, albeit on a distorted domain in the mapped plane. With this transformation, the primary solution variable, such as the temperature, must remain unchanged at corresponding points on the physical and mapped plane. The value of its normal gradient across the boundary can be obtained via, Shiah and Tan (1998),

$$\frac{d\Theta}{dn} = (\Theta_{,\underline{1}}F_{11} + \Theta_{,\underline{2}}F_{21})\, n_1 + (\Theta_{,\underline{1}}F_{12} + \Theta_{,\underline{2}}F_{22})\, n_2$$
$$\frac{d\Theta}{d\hat{n}} = \left(\Theta_{,1}F^{-1}_{11} + \Theta_{,2}F^{-1}_{21}\right)\hat{n}_1 + \left(\Theta_{,1}F^{-1}_{12} + \Theta_{,2}F^{-1}_{22}\right)\hat{n}_2 \tag{6}$$

where n_i and $\hat{n}_i$ denote components of the unit outward normal vector on the domain boundary defined in the physical and in the mapped domain, respectively; and the underline refers to the mapped plane defined by the $\hat{x}_i$ coordinate system. Following the same transformation described above, the anisotropic field involving internal concentrated heat source can be written in the mapped plane as

$$\Theta_{,\underline{ii}} = -\sum_{m=1}^{n} S'_m \delta'_m(\hat{p} - \hat{M}_m) \tag{7}$$

In Eq. (7), S'_m, denotes the equivalent source intensity in the mapped plane and is given by

$$S'_m = S_m K_{11}/\Delta \tag{8}$$

The steps to reduce the anisotropic problem to an "isotropic" one have now been presented. Its numerical solution by the BEM is briefly reviewed next.

As is well established in the BEM literature, the temperature change Θ and its normal gradient q (=$d\Theta/dn$) along the boundary of a solution domain are related by the following boundary integral equation written for the mapped plane which is indicated by the hat sign on the symbols,

$$c(\hat{P})\,\Theta(\hat{P}) = \int_{\hat{S}} q(\hat{Q})\, W(\hat{P},\hat{Q})\, d\hat{S}(\hat{Q})$$
$$- \int_{\hat{S}} \Theta(\hat{Q}) V(\hat{P},\hat{Q})\, d\hat{S}(\hat{Q}) - \sum_{m=1}^{n} S'_m W(\hat{P},\hat{M}_m) \tag{9}$$

where $\hat{P}$ and $\hat{Q}$ are the source and field point on the distorted boundary $\hat{S}$. In Eq. (9), the value of $c(\hat{P})$ depends on the geometry at $\hat{P}$; $W(\hat{P},\hat{Q})$ and $V(\hat{P},\hat{Q})$ represent the fundamental solutions for the temperature and its normal gradient, respectively, viz.

$$W(\hat{P},\hat{Q}) = \frac{1}{2\pi}\ln\left(\frac{1}{\hat{r}}\right) \quad , \quad V(\hat{P},\hat{Q}) = \frac{-1}{2\pi\hat{r}}\hat{r}_{,\underline{i}}\hat{n}_{\underline{i}} \tag{10}$$

where $\hat{r}$ represents the distance between $\hat{P}$ and $\hat{Q}$. To solve Eq. (9), the solution domain is discretized into an assemblage of line elements, each of which is defined by a finite number of nodes. Writing Eq. (9) for each of these distinct nodes with the appropriate shape functions for the interpolation of the solution variables will result in a set of simultaneous equations for the unknown temperature or its normal gradient at all the nodes. Note, however, that the collocation process for solving this boundary integral equation needs to be carried out on the distorted boundary. The input Neumann boundary conditions must therefore be accordingly transformed, as follows,

$$\frac{d\Theta}{d\hat{n}} = \left(\frac{\partial\Theta}{\partial x_1}\frac{K_{11}}{\sqrt{\Delta}} + \frac{\partial\Theta}{\partial x_2}\frac{K_{12}}{\sqrt{\Delta}}\right)\hat{n}_{\underline{1}} + \left(\frac{\partial\Theta}{\partial x_2}\right)\hat{n}_{\underline{2}} \tag{11}$$

With properly posed boundary conditions, the set of simultaneous equations for the unknown temperatures or the normal temperature gradients at nodal points may now be solved using standard matrix methods. The solved potential gradients need to be further processed, however, to obtain the corresponding values in the actual physical domain by the operation below,

$$\frac{d\Theta}{dn} = \hat{\boldsymbol{\phi}}^T \mathbf{F} \frac{\mathbf{F}^T\hat{\mathbf{n}}^T}{|\mathbf{F}^T\hat{\mathbf{n}}|} \tag{12}$$

where $\hat{\mathbf{n}}$ is the outward normal vector on the boundary of the mapped domain, expressed in terms of its components $\hat{n}_{\underline{i}}$ in the $\hat{x}_{\underline{i}}$-direction. Also, $\hat{\boldsymbol{\phi}}$ is the temperature gradient along the mapped boundary, as defined by

$$\hat{\boldsymbol{\phi}} = \begin{pmatrix} \dfrac{\partial\Theta}{\partial\hat{x}_{\underline{1}}} & \dfrac{\partial\Theta}{\partial\hat{x}_{\underline{2}}} \end{pmatrix} \tag{13}$$

and it can be directly computed using

$$\hat{\boldsymbol{\phi}}^T = \begin{pmatrix} \dfrac{\partial\Theta}{\partial\hat{x}_{\underline{1}}} \\ \\ \dfrac{\partial\Theta}{\partial\hat{x}_{\underline{2}}} \end{pmatrix} = \begin{pmatrix} \hat{s}_{\underline{1}} & \hat{s}_{\underline{2}} \\ \\ \hat{n}_{\underline{1}} & \hat{n}_{\underline{2}} \end{pmatrix}^{-1} \begin{pmatrix} \dfrac{\partial\Theta}{\partial\hat{s}} \\ \\ \dfrac{\partial\Theta}{\partial\hat{n}} \end{pmatrix} \tag{14}$$

where $\hat{s}_{\underline{i}}$ denotes the components of the unit tangential vector along the path $\hat{s}$. In Eq. (14), the temperature gradient $\frac{\partial\Theta}{\partial\hat{n}}$ is directly obtained from the solution of the BIE for the distorted domain, while the other temperature gradient $\frac{\partial\Theta}{\partial\hat{s}}$ can be computed using the standard numerical interpolation scheme involving the shape functions. Once the heat conduction problem is solved, the associated stress field can now be determined, as described below.

3 The BEM for 2D Thermoelasticity with Concentrated Heat sources

In the direct formulation of the BEM for a plane anisotropic elastic medium, the displacements, u_i, and the tractions, t_i, on the boundary S of the domain Ω are related by

$$C_{ij}(P)u_i(P) + \int_S u_i(Q)\,T_{ij}(P,Q)dS = \int_S t_i(Q)\,U_{ij}(P,Q)dS + \int_\Omega X_i(q)\,U_{ij}(P,q)d\Omega \tag{15}$$

which Q and q represent the field points on the boundary S and in the domain Ω, respectively, and P represents the source point on S. In Eq. (15), C_{ij} are the coefficients associated with boundary geometry at the source point P; and X_i represents the equivalent body-force term due to the temperature change in the domain. Also $U_{ij}(P, q)$ is the corresponding fundamental solution for displacements and is given by

$$U_{ij}(P,q) = 2Re\{r_{i1}A_{j1}\log z_1 + r_{i2}A_{j2}\log z_2\} \tag{16}$$

where r_{ij} and A_{ji} are material constants, expressed by complex quantities, $Re\{\}$ is the operator which takes the real part of the quantities in the parentheses, and z_i is a generalized complex variable. The generalized complex variable is defined in terms of the characteristic roots, μ_i and the difference of coordinates between the field point $Q(x_1, x_2)$ and the load or source point $P(x_{p1}, x_{p2})$ as follows

$$z_i = (x_1 - x_{p1}) + \mu_i(x_2 - x_{p2}) = \zeta_1 + \mu_i\zeta_2 \tag{17}$$

where ζ_i represent the local coordinates with the origin located at the source point. Also in Eq. (15), $T_{ij}(P,Q)$ is the fundamental solution for tractions, the explicit form of which is well established in the BEM literature. Since $T_{ij}(P,Q)$ is not involved in the formulation of what follows, its full expression is not repeated here.

In Eq. (16), the equivalent body-force X_i can then be written as $X_i = -\gamma_{ij}\Theta_{,j}$ where γ_{ij} are the coefficients given by $\gamma_{ij} = c_{ijkl}\alpha_{kl}$; c_{ijkl} and α_{kl} are the stiffness matrix coefficients and the coefficients of thermal expansion, respectively. With this term and the additional thermal traction term substituted into Eq. (17), the complete integral equation, when thermal effects are considered, can now be expressed as

$$C_{ij}\,u_i(P) + \int_S u_i(Q)\,T_{ij}(P,Q)dS = \int_S t_i(Q)\,U_{ij}(P,Q)dS + \int_S \gamma_{ik}\,n_k\,\Theta(Q)\,U_{ij}(P,Q)dS - \int_\Omega \gamma_{ik}\,\Theta_{,k}(q)\,U_{ij}(P,q)d\Omega \tag{18}$$

As has been presented by Shiah and Tan (1999a), the last term on the right-hand-side of Eq. (18), which is a domain integral (and will be denoted by *VI*), can be rewritten in the mapped plane defined by Eq. (4), as

$$VI_j = -\int_\Omega \gamma_{ik}\,\Theta_{,k}(q)\,U_{ij}(P,q)d\Omega = -\int_{\hat{\Omega}} \gamma_{\underline{ik}}\,\Theta_{,\underline{k}}(\hat{q})\,U_{\underline{ij}}(\hat{P},\hat{q})\,d\hat{\Omega} \tag{19}$$

where the invariant coefficients $\gamma_{\underline{ij}}$ are elements of the matrix

$$\gamma_{\underline{ik}} = \begin{pmatrix} \gamma_{11} & \dfrac{-\gamma_{11}k_{12} + \gamma_{12}k_{11}}{\sqrt{\Delta}} \\ \\ \gamma_{21} & \dfrac{-\gamma_{21}k_{12} + \gamma_{22}k_{11}}{\sqrt{\Delta}} \end{pmatrix} \tag{20}$$

To ensure that only the boundary of the solution domain needs to be modeled in the BEM analysis, the volume

integral needs to be transformed into boundary ones. For such a transformation, however, the integrand must be analytic everywhere. By making spatial differentiation of Eq, (9), the temperature gradient, $\Theta_{,\underline{k}}$, at an arbitrary point in the mapped domain is

$$\Theta_{,\underline{k}}(\hat{p}) = \int_{\hat{S}} q(\hat{Q})\, W_{\underline{k}}(\hat{p},\hat{Q})\, d\hat{S}(\hat{Q}) - \int_{\hat{S}} \Theta(\hat{Q}) V_{,\underline{k}}(\hat{p},\hat{Q})\, d\hat{S}(\hat{Q}) - \sum_{m=1}^{n} S'_m W_{,\underline{k}}(\hat{p},\hat{M}_m) = b_k(\hat{p},\hat{Q}) - \sum_{m=1}^{n} S'_m W_{,\underline{k}}(\hat{p},\hat{M}_m) \tag{21}$$

where $b_k(\hat{p},\hat{Q})$ represents the bounded value given by

$$b_k(\hat{p},\hat{Q}) = \int_{\hat{S}} q(\hat{Q})\, W_{,\underline{k}}(\hat{p},\hat{Q})\, d\hat{S}(\hat{Q}) - \int_{\hat{S}} \Theta(\hat{Q}) V_{,\underline{k}}(\hat{p},\hat{Q})\, d\hat{S}(\hat{Q}) \tag{22}$$

and the function $W_{,\underline{k}}(\hat{p},\hat{M}_m)$ is

$$W_{,\underline{k}}(\hat{p},\hat{M}_m) = \frac{(\hat{x}_k^{(\hat{p})} - \hat{x}_k^{(\hat{M}_m)})}{2\pi \hat{r}^2} \tag{23}$$

In arriving at Eq. (21), the coefficient $c(\hat{P})$ appearing in Eq. (9) has the value of unity and is dropped for the interior point solution. There are evidently singularities at the internal heat source points when $\hat{r} = 0$ and $\hat{x}_k^{(\hat{M}_m)} = \hat{x}_k^{(\hat{p})}$. When substituting Eq. (21) into Eq. (19), it is also apparent that the integral transformation process cannot be carried out unless these singularities are analytically removed. To this end, the distorted domain is sub-divided into several parts as shown in Fig. 1, where the main sub-domain $\hat{\Omega}_0$ is free of singularity and each circular sub-region, $\hat{\Omega}_m$, contains a concentrated heat source located at its center $\hat{M}_m$.

Therefore, the domain integral can be expressed as

$$VI_j = VI_j^{(\hat{\Omega}_0)} + \sum_{m=1}^{n} VI_j^{(\hat{\Omega}_m)} = -\int_{\hat{\Omega}_0} \gamma_{\underline{ik}} \Theta_{,\underline{k}}(\hat{q})\, U_{\underline{ij}}(\hat{P},\hat{q})\, d\hat{\Omega} - \sum_{m=1}^{n} \int_{\hat{\Omega}_m} \gamma_{\underline{ik}} \Theta_{,\underline{k}}(\hat{q})\, U_{\underline{ij}}(\hat{P},\hat{q})\, d\hat{\Omega} \tag{24}$$

It is necessary now to examine the volume integral for each circular sub-region, denoted by $VI_j^{(\hat{\Omega}_m)}$, when its radius is reduced to zero by following the usual limiting

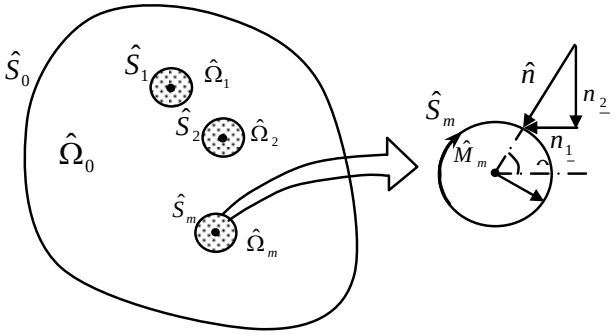

Figure 1 : A discrete distribution of concentrated heat sources in the mapped plane

process. Substituting Eq. (21) into the last term in Eq. (24) and taking the limit for the radius yields

$$VI_j^{(\hat{\Omega}_m)} = -\int_{\hat{\Omega}_m} \gamma_{\underline{ik}} \Theta_{,\underline{k}}(\hat{q})\, U_{\underline{ij}}(\hat{P},\hat{q})\, d\hat{\Omega} = \lim_{\rho\to 0} -\int_0^{2\pi}\int_0^{\rho} \gamma_{\underline{ik}} \left[b_k(\hat{q},\hat{Q}) - \sum_{m=1}^{n} S'_m W_{,\underline{k}}(\hat{q},\hat{M}_m) \right] \cdot U_{\underline{ij}}(\hat{P},\hat{q})\, r\, dr\, d\theta \tag{25}$$

The term associated with the bounded value, $b_k(\hat{q},\hat{Q})$, vanishes when the radius ρ approaches zero. It follows that the volume integral can be expressed as

$$VI_j^{(\hat{\Omega}_m)} = \lim_{\rho\to 0} \int_0^{2\pi}\int_0^{\rho} \gamma_{\underline{ik}} \sum_{m=1}^{n} \frac{S'_m (\hat{x}_k^{(\hat{M}_m)} - \hat{x}_k^{(\hat{q})})}{2\pi \left[(\hat{x}_1^{(\hat{M}_m)} - \hat{x}_1^{(\hat{q})})^2 + (\hat{x}_2^{(\hat{M}_m)} - \hat{x}_2^{(\hat{q})})^2 \right]} \cdot U_{\underline{ij}}(\hat{P},\hat{q})\, r\, dr\, d\theta \tag{26}$$

When the interior field point $\hat{q}$ does not fall inside the same sub-region where the m-th heat source point $\hat{M}_m$ is located, the associated volume integral vanishes. Thus, the above volume integral turns out to be

$$VI_j^{(\hat{\Omega}_m)} = \lim_{\rho\to 0} \int_0^{2\pi}\int_0^{\rho} \frac{-S'_m(\gamma_{\underline{i1}} r\cos\theta + \gamma_{\underline{i2}} r\sin\theta)}{2\pi r^2} \cdot U_{\underline{ij}}(\hat{P},\hat{M}_m)\, r\, dr\, d\theta = -\frac{S'_m}{2\pi} U_{\underline{ij}}(\hat{P},\hat{M}_m) \lim_{\rho\to 0} \int_0^{2\pi}\int_0^{\rho} (\gamma_{\underline{i1}}\cos\theta + \gamma_{\underline{i2}}\sin\theta)\, dr\, d\theta = 0 \tag{27}$$

Therefore Eq. (24) becomes just

$$VI_j = -\int_{\hat{\Omega}_0} \gamma_{\underline{ik}}\,\Theta_{,\underline{k}}(\hat{q})\,U_{\underline{ij}}(\hat{P},\hat{q})\,d\hat{\Omega} \tag{28}$$

With singularities removed in the mapped domain, the volume integral may now be transformed to boundary ones by applying Green's theorem. The transformed volume integral of Eq. (28) can be written as

$$\begin{aligned}\mathrm{VI_j} = &-\int_{\hat{S}} \gamma_{\underline{ik}}\,U_{\underline{ij}}(\hat{P},\hat{Q})\Theta(\hat{Q})\,n_{\underline{k}}\,d\hat{S}\\ &+\int_{\hat{S}} (\gamma_{\underline{ik}}\,Q_{\underline{ijk},\underline{t}}(\hat{P},\hat{Q})\Theta(\hat{Q})\\ &-\gamma_{\underline{ik}}\,Q_{\underline{ijk}}(\hat{P},\hat{Q})\,\Theta_{,\underline{t}}(\hat{Q}))\,n_{\underline{t}}\,d\hat{S}\\ &+\int_{\hat{\Omega}_0} \gamma_{\underline{ik}}\,Q_{\underline{ijk}}(\hat{P},\hat{q})\Theta_{\underline{tt}}(\hat{q})\,d\hat{\Omega}\end{aligned} \tag{29}$$

where $Q_{\underline{ijk}}$ and $Q_{\underline{ijk},\underline{t}}$ are defined by

$$\begin{aligned}&Q_{\underline{ijk}}\\ &= 2Re\left\{\frac{r_{i1}A_{j1}\mu_{\underline{k1}}z_{\underline{1}}\log(z_{\underline{1}})}{(\mu_{\underline{11}}{}^2+\mu_{\underline{21}}{}^2)}+\frac{r_{i2}A_{j2}\mu_{\underline{k2}}z_{\underline{2}}\log(z_{\underline{2}})}{(\mu_{\underline{21}}{}^2+\mu_{\underline{22}}{}^2)}\right\}\end{aligned} \tag{30}$$

$$\begin{aligned}Q_{\underline{ijk},\underline{t}} = 2Re\Bigg\{&\frac{r_{i1}A_{j1}\mu_{\underline{k1}}\mu_{\underline{t1}}(1+\log(z_{\underline{1}}))}{(\mu_{\underline{11}}{}^2+\mu_{\underline{21}}{}^2)}\\ &+\frac{r_{i2}A_{j2}\mu_{\underline{k2}}\mu_{\underline{t2}}(1+\log(z_{\underline{2}}))}{(\mu_{\underline{21}}{}^2+\mu_{\underline{22}}{}^2)}\Bigg\}\end{aligned} \tag{31}$$

In Eqs. (30) and (31), the coefficients $\mu_{\underline{ji}}$ are given by

$$\mu_{\underline{ji}} = \begin{pmatrix} \frac{K_{11}+\mu_1 K_{12}}{\sqrt{\Delta}} & \frac{K_{11}+\mu_2 K_{12}}{\sqrt{\Delta}} \\ \mu_1 & \mu_2 \end{pmatrix} \tag{32}$$

From Eq. (7), it is clear that the last term in Eq. (29) is zero, since the interior point $\hat{q}$ is in the sub-region $\hat{\Omega}_0$ which is free of concentrated heat sources. However the boundary integrals in Eq. (29) need to be performed along all surfaces of the sub-region $\hat{\Omega}_0$, including the outside boundary $\hat{S}_0$ and those inside $\hat{S}_1, \ldots, \hat{S}_m$ as shown in Fig. 1. By noting that the directions of the integration paths are opposite for the inside and the outside surfaces, Eq. (29) can be rewritten as

$$\begin{aligned}\mathrm{VI_j} = &-\int_{\hat{S}_0} \gamma_{\underline{ik}}\,U_{\underline{ij}}(\hat{P},\hat{Q})\Theta(\hat{Q})\,n_{\underline{k}}\,d\hat{S}\\ &+\lim_{\rho\to 0}\sum_{m=1}^{n}\int_{\hat{S}_m} \gamma_{\underline{ik}}\,U_{\underline{ij}}(\hat{P},\hat{q})\Theta(\hat{q})\,n_{\underline{k}}\,(\rho\,d\theta)\\ &+\int_{\hat{S}_0} \gamma_{\underline{ik}}\,Q_{\underline{ijk},\underline{t}}(\hat{P},\hat{Q})\Theta(\hat{Q})\,n_{\underline{t}}\,d\hat{S}\\ &-\lim_{\rho\to 0}\sum_{m=1}^{n}\int_{\hat{S}_m} \gamma_{\underline{ik}}\,Q_{\underline{ijk},\underline{t}}(\hat{P},\hat{q})\Theta(\hat{q})\,n_{\underline{t}}\,(\rho\,d\theta)\\ &-\int_{\hat{S}_0} \gamma_{\underline{ik}}\,Q_{\underline{ijk}}(\hat{P},\hat{Q})\,\Theta_{,\underline{t}}(\hat{Q})\,n_{\underline{t}}\,d\hat{S}\\ &+\lim_{\rho\to 0}\sum_{m=1}^{n}\int_{\hat{S}_m} \gamma_{\underline{ik}}\,Q_{\underline{ijk}}(\hat{P},\hat{q})\,\Theta_{,\underline{t}}(\hat{q})\,n_{\underline{t}}\,(\rho\,d\theta)\end{aligned} \tag{33}$$

To evaluate the first two limiting terms in Eq. (33), consider for the moment the temperature field $\Theta(\hat{q})$ at the interior, given by

$$\begin{aligned}\Theta(\hat{q}) = &\int_{\hat{S}_0} q\,(\hat{Q})\,W(\hat{q},\hat{Q})\,d\hat{S}\\ &-\int_{\hat{S}_0}\Theta\,(\hat{Q})V(\hat{q},\hat{Q})\,d\hat{S}-\sum_{m=1}^{n} S'_m W(\hat{q},\hat{M}_m) = bo(\hat{q},\hat{Q})\\ &-\sum_{m=1}^{n}\frac{S'_m}{2\pi}\log\frac{1}{\sqrt{(\hat{x}_1^{(\hat{M}_m)}-\hat{x}_1^{(\hat{q})})^2+(\hat{x}_2^{(\hat{M}_m)}-\hat{x}_2^{(\hat{q})})^2}}\end{aligned} \tag{34}$$

where $b_o(\hat{q},\hat{Q})$ denotes the bounded value computed by

$$\begin{aligned}&b_o(\hat{q},\hat{Q})\\ &=\int_{\hat{S}_0} q\,(\hat{Q})\,W(\hat{q},\hat{Q})\,d\hat{S}-\int_{\hat{S}_0}\Theta\,(\hat{Q})V(\hat{q},\hat{Q})\,d\hat{S}\end{aligned} \tag{35}$$

As seen earlier above, the singularity exists only when the interior point $\hat{q}$ coincides with the heat source point. With reference to Figure 2, Eq. (34) can be further re-

written as

$$\begin{aligned}\Theta(\hat{q}) &= \int_{\hat{S}_0} q(\hat{Q}) W(\hat{q},\hat{Q})\, d\hat{S} \\ &\quad - \int_{\hat{S}_0} \Theta(\hat{Q}) V(\hat{q},\hat{Q})\, d\hat{S} - \sum_{m=1}^{n} S'_m W(\hat{q},\hat{M}_m) \\ &= b_0(\hat{q},\hat{Q}) \\ &\quad - \sum_{m=1}^{n} \frac{S'_m}{2\pi} \log \frac{1}{\sqrt{(\hat{x}_1^{(\hat{M}_m)} - \hat{x}_1^{(\hat{q})})^2 + (\hat{x}_2^{(\hat{M}_m)} - \hat{x}_2^{(\hat{q})})^2}} \\ &= b_0(\hat{q},\hat{Q}) \\ &\quad - \sum_{m=1}^{k-1} \frac{S'_m}{2\pi} \log \frac{1}{\sqrt{(\hat{x}_1^{(\hat{M}_m)} - \hat{x}_1^{(\hat{q})})^2 + (\hat{x}_2^{(\hat{M}_m)} - \hat{x}_2^{(\hat{q})})^2}} \\ &\quad - \sum_{m=k+1}^{n} \frac{S'_m}{2\pi} \log \frac{1}{\sqrt{(\hat{x}_1^{(\hat{M}_m)} - \hat{x}_1^{(\hat{q})})^2 + (\hat{x}_2^{(\hat{M}_m)} - \hat{x}_2^{(\hat{q})})^2}} \\ &\quad - \frac{S'_k}{2\pi} \log \frac{1}{\sqrt{(\hat{x}_1^{(\hat{M}_k)} - \hat{x}_1^{(\hat{q})})^2 + (\hat{x}_2^{(\hat{M}_k)} - \hat{x}_2^{(\hat{q})})^2}} \\ &= B_0(\hat{q},\hat{Q}) - \frac{S'_k}{2\pi} \log \frac{1}{\sqrt{(\hat{x}_1^{(\hat{M}_k)} - \hat{x}_1^{(\hat{q})})^2 + (\hat{x}_2^{(\hat{M}_k)} - \hat{x}_2^{(\hat{q})})^2}} \\ &= B_o(\hat{q},\hat{Q}) + \frac{S'_k}{2\pi} \log \rho \end{aligned} \tag{36}$$

where $B_o(\hat{q},\hat{Q})$ represents the bounded value from

$$\begin{aligned} B_0(\hat{q},\hat{Q}) &= b_0(\hat{q},\hat{Q}) \\ &\quad - \sum_{m=1}^{k-1} \frac{S'_m}{2\pi} \log \frac{1}{\sqrt{(\hat{x}_1^{(\hat{M}_m)} - \hat{x}_1^{(\hat{q})})^2 + (\hat{x}_2^{(\hat{M}_m)} - \hat{x}_2^{(\hat{q})})^2}} \\ &\quad - \sum_{m=k+1}^{n} \frac{S'_m}{2\pi} \log \frac{1}{\sqrt{(\hat{x}_1^{(\hat{M}_m)} - \hat{x}_1^{(\hat{q})})^2 + (\hat{x}_2^{(\hat{M}_m)} - \hat{x}_2^{(\hat{q})})^2}} \end{aligned} \tag{37}$$

By substituting Eq. (36) into Eq. (33) and taking the limit as ρ approaches zero, it can be verified that

$$\begin{aligned} &\lim_{\rho\to 0} \sum_{m=1}^{n} \int_{\hat{S}_m} \gamma_{\underline{ik}} U_{\underline{ij}}(\hat{P},\hat{q}) \left(B_o(\hat{q},\hat{Q}) + \frac{S'_m}{2\pi} \log \rho \right) n_{\underline{k}}(\rho\, d\theta) \\ &= 0 \end{aligned} \tag{38}$$

and

$$\begin{aligned} &\lim_{\rho\to 0} \sum_{m=1}^{n} \int_{\hat{S}_m} \gamma_{\underline{ik}} Q_{\underline{ijk},\underline{t}}(\hat{P},\hat{q}) \left(B_o(\hat{q},\hat{Q}) + \frac{S'_m}{2\pi} \log \rho \right) n_{\underline{t}}(\rho\, d\theta) \\ &= 0 \end{aligned} \tag{39}$$

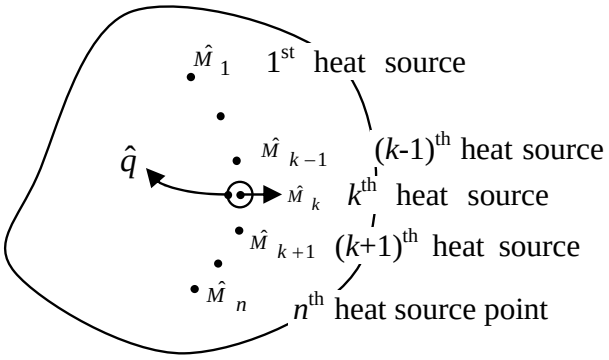

Figure 2 : A domain with n concentrated heat sources

The remaining task in the transformation process is to evaluate the last limiting term in Eq. (33). Substitution of Eq. (21) into this term results in

$$\begin{aligned} &\lim_{\rho\to 0} \sum_{m=1}^{n} \int_{\hat{S}_m} \gamma_{\underline{ik}} Q_{\underline{ijk}}(\hat{P},\hat{q})\, \Theta_{,\underline{t}}(\hat{q})\, n_{\underline{t}}(\rho\, d\theta) \\ &= \lim_{\rho\to 0} \sum_{m=1}^{n} \int_{\hat{S}_m} \gamma_{\underline{ik}} Q_{\underline{ijk}}(\hat{P},\hat{q}) \\ &\quad \left[\begin{array}{l} \left(b_1(\hat{q},\hat{Q}) - \sum\limits_{m=1}^{n} S'_m W_{,\underline{1}}(\hat{q},\hat{M}_m) \right) \cos\theta \\ + \left(b_2(\hat{q},\hat{Q}) - \sum\limits_{m=1}^{n} S'_m W_{,\underline{2}}(\hat{q},\hat{M}_m) \right) \sin\theta \end{array} \right] (\rho\, d\theta) \end{aligned} \tag{40}$$

Due to the fact that $W_{,\underline{t}}(\hat{q},\hat{M}_m)$ is singular only when the point $\hat{q}$ is on the surface of $\hat{S}_m$ and as it becomes coincident with $\hat{M}_m$, Eq. (40) can be re-written as

$$\begin{aligned} &\lim_{\rho\to 0} \sum_{m=1}^{n} \int_{\hat{S}_m} \gamma_{\underline{ik}} Q_{\underline{ijk}}(\hat{P},\hat{q})\, \Theta_{,\underline{t}}(\hat{q})\, n_{\underline{t}}(\rho\, d\theta) \\ &= \lim_{\substack{\rho\to 0 \\ \hat{q}\to\hat{M}_m}} \sum_{m=1}^{n} \int_{\hat{S}_m} \gamma_{\underline{ik}} Q_{\underline{ijk}}(\hat{P},\hat{M}_m) \\ &\quad \left[\begin{array}{l} \left(B_1(\hat{M}_m,\hat{Q}) - S'_m W_{,\underline{1}}(\hat{q},\hat{M}_m) \right) \cos\theta \\ + \left(B_2(\hat{M}_m,\hat{Q}) - S'_m W_{,\underline{2}}(\hat{q},\hat{M}_m) \right) \sin\theta \end{array} \right] (\rho\, d\theta) \end{aligned} \tag{41}$$

where $B_t(\hat{M}_m,\hat{Q})$ represents the bounded part of $\lim\limits_{\hat{q}\to\hat{M}_m} \left(b_t(\hat{q},\hat{Q}) - \sum\limits_{m=1}^{n} S'_m W_{,\underline{t}}(\hat{q},\hat{M}_m) \right)$. It can be easily verified that the all the bounded values of the integrals of Eq. (41) vanish when ρ approaches zero. With reference to Fig.1 which shows the outward normal vector $\hat{n}$

pointing towards the center of the circle of exclusion, Eq. (41) may be further re-written using Eq. (23) to give

$$\begin{aligned}
&\lim_{\rho\to 0}\sum_{m=1}^{n}\int_{\hat{S}_m}\gamma_{\underline{ik}}\,Q_{\underline{ijk}}(\hat{P},\hat{q})\,\Theta_{,\underline{t}}(\hat{q})\,n_{\underline{t}}(\rho\,d\theta)\\
&=\lim_{\rho\to 0}\sum_{m=1}^{n}\int_{0}^{2\pi}\gamma_{\underline{ik}}\,Q_{\underline{ijk}}(\hat{P},\hat{M}_m)\\
&\qquad\left[\begin{array}{l}\left(S'_m\frac{(\hat{x}_1^m-\hat{x}_1^M)}{2\pi\rho^2}\right)(-\cos\theta)\\ +\left(-S'_m\frac{(\hat{x}_2^m-\hat{x}_2^M)}{2\pi\rho^2}\right)(-\sin\theta)\end{array}\right](\rho\,d\theta)
\end{aligned}\tag{42}$$

Along the path of integration $\hat{S}_m$, the coordinates of the field point $\hat{q}$ are given by

$$\hat{x}_1^m=\hat{x}_1^M+\rho\cos\theta\quad,\quad\hat{x}_2^m=\hat{x}_2^M+\rho\sin\theta\tag{43}$$

Therefore, Eq. (42) becomes

$$\begin{aligned}
&\lim_{\rho\to 0}\sum_{m=1}^{n}\int_{\hat{S}_m}\gamma_{\underline{ik}}\,Q_{\underline{ijk}}(\hat{P},\hat{q})\,\Theta_{,\underline{t}}(\hat{q})\,n_{\underline{t}}(\rho\,d\theta)\\
&=\lim_{\rho\to 0}\sum_{m=1}^{n}\int_{0}^{2\pi}\gamma_{\underline{ik}}\,Q_{\underline{ijk}}(\hat{P},\hat{q})\\
&\quad\left[\left(S'_m\frac{\rho\cos\theta}{2\pi\rho^2}\right)(-\cos\theta)\right.\\
&\qquad\left.+\left(S'_m\frac{\rho\sin\theta}{2\pi\rho^2}\right)(-\sin\theta)\right](\rho\,d\theta)\\
&=-\sum_{m=1}^{n}\int_{0}^{2\pi}\gamma_{\underline{ik}}\,Q_{\underline{ijk}}(\hat{P},\hat{M}_m)\left(\frac{S'_m}{2\pi}\right)d\theta\\
&=-\sum_{m=1}^{n}S'_m\,\gamma_{\underline{ik}}\,Q_{\underline{ijk}}(\hat{P},\hat{M}_m)
\end{aligned}\tag{44}$$

The volume-surface-integral transformation for the thermal effects is now complete. The extra volume integral seen in Eq. (19) can now be computed via

$$\begin{aligned}
\mathrm{VI_j}=&-\int_{\hat{S}_0}\gamma_{\underline{ik}}\,U_{\underline{ij}}(\hat{P},\hat{Q})\Theta(\hat{Q})\,n_{\underline{k}}\,d\hat{S}\\
&+\int_{\hat{S}_0}\gamma_{\underline{ik}}\,Q_{\underline{ijk},\underline{t}}(\hat{P},\hat{Q})\Theta(\hat{Q})\,n_{\underline{t}}\,d\hat{S}\\
&-\int_{\hat{S}_0}\gamma_{\underline{ik}}\,Q_{\underline{ijk}}(\hat{P},\hat{Q})\,\Theta_{,\underline{t}}(\hat{Q})\,n_{\underline{t}}\,d\hat{S}\\
&-\sum_{m=1}^{n}S'_m\,\gamma_{\underline{ik}}\,Q_{\underline{ijk}}(\hat{P},\hat{M}_m)
\end{aligned}\tag{45}$$

For many practical applications, concentrated heat sources are often placed at the surface of the domain. The formulation developed above can also be modified for BEM modeling of these problems. For this purpose, consider a concentrated heat source located at a corner with an included angle λ as shown in Fig. 3. The foregoing process to exclude the singularity at the point of the heat source is still valid, provided the term in Eq. (44) is modified by

$$\begin{aligned}
&\lim_{\rho\to 0}\sum_{m=1}^{n}\int_{\hat{S}_m}\gamma_{\underline{ik}}\,Q_{\underline{ijk}}(\hat{P},\hat{q})\,\Theta_{,\underline{t}}(\hat{q})\,n_{\underline{t}}(\rho\,d\theta)\\
&=-\sum_{m=1}^{n}\int_{\theta_1}^{\theta_2}\gamma_{\underline{ik}}\,Q_{\underline{ijk}}(\hat{P},\hat{M}_m)\left(\frac{S'_m}{2\pi}\right)d\theta\\
&=-\sum_{m=1}^{n}S'_m\,\gamma_{\underline{ik}}\,Q_{\underline{ijk}}(\hat{P},\hat{M}_m)\,(\lambda_m/2\pi)
\end{aligned}\tag{46}$$

It should be reminded that the included angle between the two planes meeting at the corner is defined in the mapped plane; it can be readily computed using the outward normal vectors at the corner of the two adjacent boundary elements. Although this modification to remove the singularity of the integrals is fundamentally valid for point heat sources on the boundary, care should still be exercised when modeling the problem. Some difficulties may arise in the direct numerical evaluation of the logarithmic function in $Q_{\underline{ijk}}(\hat{P},\hat{M}_m)$ when the distance between points $\hat{P}$ and $\hat{M}_m$ becomes zero in the collocation. A simple way to avoid this is to relocate the heat source to be at a point in the interior of the domain very close to the boundary. Numerical experiments conducted by the authors suggest that satisfactory results will typically be obtained if it is placed at a relative distance d/l =0.1 from the nearest element; d being the distance and l is the length of the element.

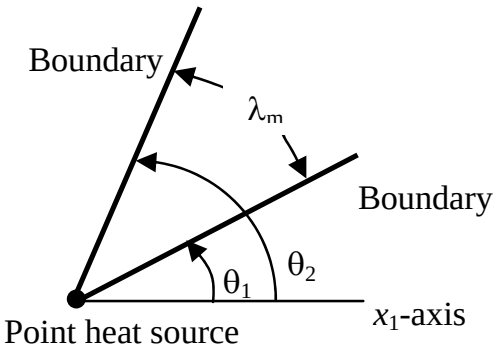

Figure 3 : Point heat source at a corner

There remains one issue that needs to be addressed for the more general case of a multiply connected domain. It concerns the terms containing $\log(z)$ in the integrands of the BIE, as it may not be analytic everywhere in the domain. This has been explained in detail in Zhang, *et al* (1996a), and Shiah and Tan (1999a). If the principal value of z is defined, as by default in computing, in the range -$\pi < arg(z) < \pi$, the quantity $\log(z)$ is not analytic along the negative ζ_1-axis as shown in Fig.4. This will invalidate the foregoing volume-to-surface integral transformation. Although the problem may be avoided by redefining the range of the argument, $arg(z)$, it is not always possible to do so to ensure the analyticity of $\log(z)$ everywhere in the domain. Referring to Fig. 4, if rays from any point along an inner boundary are projected in arbitrary directions, they will cut through the domain.

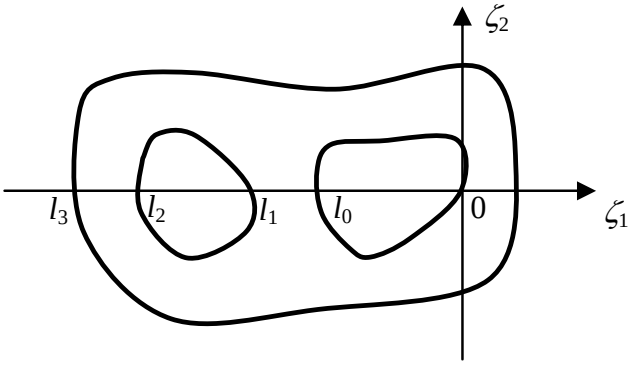

Figure 4 : A multiply connected domain

This problem was resolved by Zhang *et al* (1996b) in their BEM work for body force loading, by carrying out a limiting process. They obtained a series of extra line integrals over the intervals along the negative ζ_1-axis where it cuts the domain, such as (l_0, l_1), (l_2, l_3), from the source point on the internal surface of the region. Similarly, for the general case here, if the negative ζ_1-axis cuts through the region m times in the intervals (l_{2m-1}, l_{2m-2}), (l_{2m-3}, l_{2m-3}),....., (l_1, l_0), the complete boundary integral equation for plane anisotropic thermoelasticity involving a discrete distribution of concentrated heat sources can be expressed as

$$
\begin{aligned}
&C_{ij}\,u_i(P) + \int_S u_i(Q)\,T_{ij}(P,Q)dS \\
&= \int_S t_i(Q)\,U_{ij}(P,Q)dS + \int_S \gamma_{ik}\,n_k\,U_{ij}(P,Q)\Theta dS \\
&- \int_{\hat{S}} \gamma_{\underline{ik}}\,n_{\underline{k}}\,U_{ij}(P,Q)\Theta d\hat{S} + \int_{\hat{S}} [\gamma_{\underline{ik}}\,Q_{\underline{ijk},\underline{t}}(P,Q)\Theta \\
&- \gamma_{\underline{ik}}\,Q_{\underline{ijk}}(P,Q)\,\Theta_{,\underline{t}}]\,n_{\underline{t}}\,d\hat{S} + \sum_{n=1}^{m}\int_{l_{2n-1}}^{l_{2n-2}} L_j(\zeta_1)\,d\zeta_1 \\
&- \sum_{m=1}^{n} S'_m\,\gamma_{\underline{ik}}\,Q_{\underline{ijk}}(\hat{P},\hat{M}_m)\,(\lambda_m/2\pi)
\end{aligned}
\tag{47}
$$

In Eq. (44), the integrand, $L_j(\zeta_1)$, is given by

$$
\begin{aligned}
&L_j(\zeta_1) \\
&= -4\pi\Theta\left(\frac{K_{12}}{K_{11}}\gamma_{\underline{i1}} + \frac{\sqrt{\Delta}}{K_{11}}\gamma_{\underline{i2}}\right)\mathrm{Im}\{r_{i1}A_{j1} + r_{i2}A_{j2}\} \\
&\quad + 4\pi\Theta\gamma_{\underline{ik}}\left(\frac{K_{12}}{K_{11}}Im\left\{\frac{r_{i1}A_{j1}\mu_{\underline{11}}\mu_{\underline{k1}}}{\mu_{\underline{11}}{}^2 + \mu_{\underline{21}}{}^2} + \frac{r_{i2}A_{j2}\mu_{\underline{12}}\mu_{\underline{k2}}}{\mu_{\underline{12}}{}^2 + \mu_{\underline{22}}{}^2}\right\}\right. \\
&\quad \left. + \frac{\sqrt{\Delta}}{K_{11}}\mathrm{Im}\left\{\frac{r_{i1}A_{j1}\mu_{\underline{21}}\mu_{\underline{k1}}}{\mu_{\underline{11}}{}^2 + \mu_{\underline{21}}{}^2} + \frac{r_{i2}A_{j2}\mu_{\underline{22}}\mu_{\underline{k2}}}{\mu_{\underline{12}}{}^2 + \mu_{\underline{22}}{}^2}\right\}\right) \\
&\quad - 4\pi\ \gamma_{\underline{ik}}\left(\frac{K_{12}}{K_{11}}\Theta_{,\underline{1}} + \Theta_{,\underline{2}}\frac{\sqrt{\Delta}}{K_{11}}\right) \\
&\qquad\qquad \mathrm{Im}\left\{\frac{r_{i1}A_{j1}\mu_{\underline{k1}}}{\mu_{\underline{11}}{}^2 + \mu_{\underline{21}}{}^2} + \frac{r_{i2}A_{j2}\mu_{\underline{k2}}}{\mu_{\underline{12}}{}^2 + \mu_{\underline{22}}{}^2}\right\}
\end{aligned}
\tag{48}
$$

It should be noted, however, the problem of multi-values will also occur for $Q_{\underline{ijk}}(\hat{P},\hat{M}_m)$ appearing in the last term of Eq. (47) when a concentrated heat source is located on its branch cut, which is set by default in computing to be the negative ζ_1-axis. For a simply connected domain, this problem can always be avoided by redefining the arguments mentioned above, such that the branch cut is aligned with the outward normal vector (Zhang, *et al* (1996a)). However, for a multiply connected region, care should be taken in the boundary discretisation to ensure that the concentrated heat source does not lie on the negative ζ_1-axis. An expedient way to overcome these difficulties for multiply connected bodies in general and to avoid the evaluation of the extra line integrals of Eq. (47) is to adopt the sub-regioning scheme commonly used in BEM analysis, making each sub-region a simply connected sub-domain.

The formulations developed for treating anisotropic thermal stresses arising from concentrated heat sources in two dimensions have been implemented into an existing BEM computer code which employs quadratic isoparametric elements (e.g. Zhang, *et al* (1996b), Shiah and Tan (1999a)). Three numerical examples are provided next to demonstrate their veracity and applicability.

4 Numerical Examples

For the purpose of verification of the numerical algorithm, the first problem analyzed is an isotropic steel disc, but treated as quasi-isotropic in the BEM code for anisotropy. The material properties of the steel were taken to be as follows

E	G	ν	α	K
200	77	0.29	11.7E-6	60
Gpa	*GPa*		$/\,^0C$	$W/(m\text{-}^oC)$

where E is the elastic modulus, G the shear modulus, ν the Poisson's ratio, α the thermal expansion coefficient, and K the thermal conductivity coefficient. The second problem considered is an anisotropic rectangular plate with a discrete distribution of concentrated heat sources inside domain. The third example deals with a doubly connected domain with a concentrated heat source prescribed on the boundary. The material properties chosen in the last two examples were arbitrarily chosen to correspond to those of a glass-epoxy that is generally anisotropic. Following the usual notations but with asterisks denoting values in the directions of principal axes, the mechanical properties are listed below.

E^*_{11}/E^*_{22}	ν^*_{12}	G^*_{12}/E^*_{22}	$\eta^*_{12,1}$	$\eta^*_{12,2}$	$\alpha^*_{11}/\alpha^*_{22}$	K^*_{11}/K^*_{22}
55/21	0.25	9.7/21	0	0	6.3/20	3.46/0.35

All three problems were analyzed under the assumptions of plane stress conditions.

These example problems are also analyzed by the finite element method as a means of comparison of the numerical results. The commercial software, ANSYS, was employed. It should be mentioned that when modeling the concentrated heat source with ANSYS, a very refined mesh discretisation in its vicinity was introduced; over these elements, a uniform heat flux is prescribed. Furthermore, the anisotropic field problem was solved in the FEM analysis in a rotated, scaled, coordinate system mentioned earlier above.

4.1 Example 1

As shown in Fig. 5, the first problem treated is a quasi-isotropic thin disc with a concentrated heat source of intensity $S = 60\ W$ located at its center. The circumferential edge of the disc is fully constrained and is kept at a constant uniform temperature $T = 0°C$. Although only a sector of the disk needs to be considered, by virtue of axisymmetry, the problem was solved for the whole domain for the purpose of verification of the computer code for anisotropy. For the analysis, R was taken to be 1 m. Thirty-two quadratic line elements with a total of sixty-four nodes (Fig. 5) were used to model the problem with BEM. The associated thermal field was first solved to obtain the temperature gradients at the nodes along the circumference. For the corresponding FEM analysis with ANSYS, a total of 2654 PLANE77 (high-order quadrilateral) elements were employed; the mesh is shown in Figure 6. Table 1 shows the excellent agreement of the solutions obtained from both numerical methods for the distribution of the computed normalized temperature, $T \cdot (KR/S)$, along a radial plane of the disc. The computed normalized temperature gradients at the circumferential edge, $(dT/dn) \cdot (KR^2/S)$, were also in perfect agreement with each other to four significant digits, with a uniform value of -3.609E-2. With the thermal field obtained and using the same mesh design, the BEM thermoelastic stress analysis was then carried out. The corresponding FEM analysis using ANSYS was also performed, but with element type PLANE82 (high-order quadrilateral element for elasticity) instead. Figure 7 shows the distribution of the normalized radial stress, σ_{rr} $KR/(E\alpha S)$, at the interior points along a radial plane from the centre of the disc. Table 2 lists the computed normalized radial stress around the circumference obtained using both numerical methods. It can be seen that the agreement between the computed results is again excellent, and that the radial stress is uniform all around the circumference, as to be expected. The hoop stress at the disc circumference was also found to be uniform, the nu-

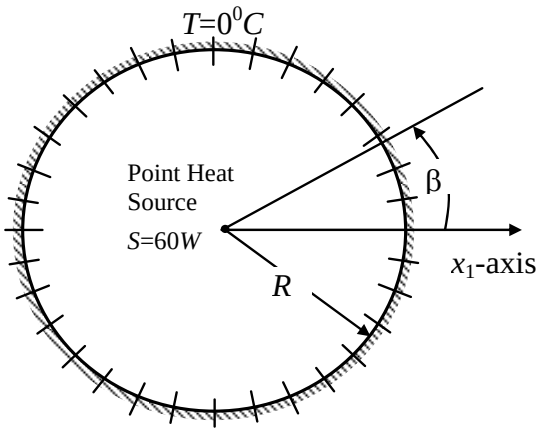

Figure 5 : A circular disc with a concentrated heat source and the BEM mesh discretisation - Example 1

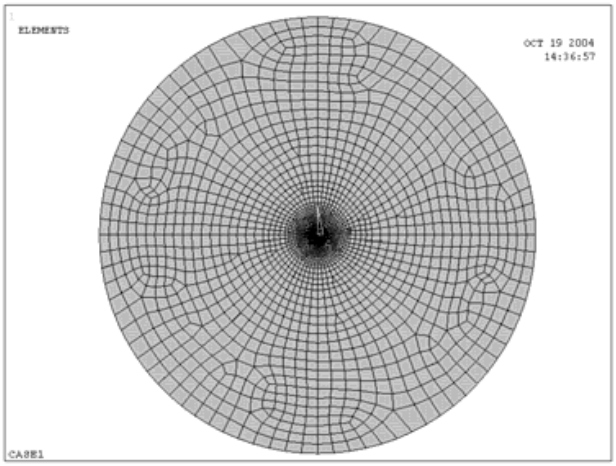

Figure 6 : FEM mesh for analysis with ANSYS - Example 1

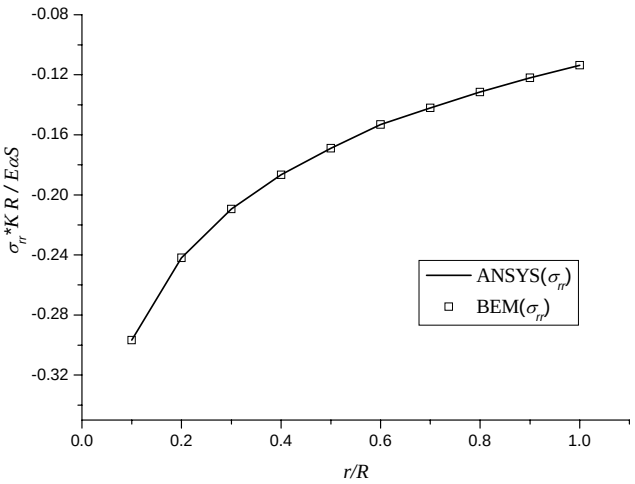

Figure 7 : Distribution of the normalized radial stress $\sigma_{rr}KR/E\alpha S$ along a radial plane – Example 1

Table 1 : Distribution of normalized temperature, $T^*(KR/S)$, along a radial plane – Example 1

r/R	$T^*(K\,R\,/\,S)$		% Diff.
	BEM quasi-isotropic	ANSYS isotropic	
0.1	0.3742	0.3742	0
0.2	0.2639	0.2639	0
0.3	0.1994	0.1994	0
0.4	0.1536	0.1536	0
0.5	0.1181	0.1181	0
0.6	0.0891	0.0891	0
0.7	0.0645	0.0645	0
0.8	0.0433	0.0433	0
0.9	0.0245	0.0245	0

merical value being in agreement with the expected value of the product of the Poisson's ratio and the radial stress.

4.2 Example 2

The second problem considered is a rectangular glass-epoxy plate ($1\ m\times\ 2\ m$) with two internal point heat sources with intensity S=100 W as shown in Fig. 8. To demonstrate the capability of the developed BEM algorithm in dealing with full anisotropy, the material principal axes are rotated counterclockwise by an angle θ measured from the x_1-axis. For the purpose of illustration, the temperature at the top and bottom surfaces remain unchanged (T=0°C), and these surfaces are fully constrained from displacement. The two perpendicular sides, on the other hand, are thermally insulated and free. The problem is investigated for different separation distances between the two heat sources, with d/L(see Fig. 8) varying from 0.1 to 0.4. Relatively refined elements were employed at those parts of the boundary close to the heat sources in the BEM model that has a

Table 2 : Normalized radial stress, $\sigma_{rr}KR/E\alpha S$, around the circumference of the disc – Example 1

β	$\sigma_{rr}KR/E\alpha S$		Diff.
	BEM quasi-isotropic	ANSYS isotropic	
0.0	-1.1394E-01	-1.1365E-01	0.3
22.5	-1.1373E-01	-1.1369E-01	0.0
45.0	-1.1386E-01	-1.1372E-01	0.1
67.5	-1.1366E-01	-1.1368E-01	0.0
90.0	-1.1372E-01	-1.1365E-01	0.1
112.5	-1.1380E-01	-1.1369E-01	0.1
135.0	-1.1367E-01	-1.1372E-01	0.0
157.5	-1.1392E-01	-1.1368E-01	0.2
180.0	-1.1403E-01	-1.1365E-01	0.3
202.5	-1.1380E-01	-1.1369E-01	0.1
225.0	-1.1324E-01	-1.1373E-01	0.4
247.5	-1.1340E-01	-1.1369E-01	0.3
270.0	-1.1358E-01	-1.1365E-01	0.1
292.5	-1.1320E-01	-1.1369E-01	0.4
315.0	-1.1375E-01	-1.1372E-01	0.0
337.5	-1.1393E-01	-1.1368E-01	0.2

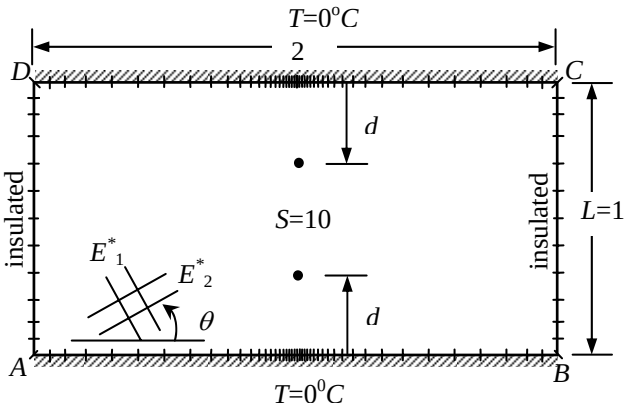

Figure 8 : A rectangular plate with a pair of concentrated heat sources in the domain – Example 2

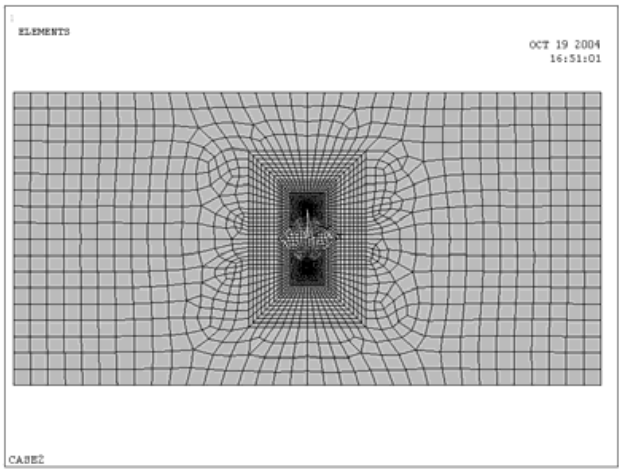

Figure 9 : FEM mesh for analysis with ANSYS – Example 2, d/L=0.4

total 116 elements. In the FEM model with ANSYS, because very refined mesh discretizations at the locations of the heat sources were required, a separate mesh was developed for each case when the heat sources were displaced. Figure 9 shows the FEM mesh used for the case of d/L=0.4, where 3353 elements were used. To investigate the anisotropic effect of the material, the problem is solved by both numerical approaches for various θ values, namely, 0°, 30°, 60°, and 90°. The computed stresses along the constrained surfaces, all normalized by the quantity, $E_{11}\alpha_{11}S/LK_{11}$, are shown in Figs. 10 to 12 for σ_{11}, σ_{22}, and σ_{12}, respectively. Comparisons of all the BEM and FEM computed stresses on the constrained surfaces again show excellent agreement of the numerical solutions with one another.

4.3 Example 3

The third problem considered is a doubly connected region of a thin square plate containing a central circular with a point heat source on the boundary, with the dimensions as shown in Fig. 13. For the purpose of demonstration, the temperature at the top surface was prescribed a value of 100°C while the bottom surface was prescribed with T=0°C; all other surfaces, including the circumference of the central hole, are thermally insulated. Also, it is assumed that a concentrated heat source with strength $S=10^3$ W exists at the top surface. The exterior boundary of the plate is constrained from displacements as shown in Fig. 13 while the edge of the central hole is free.

The problem can be solved using the conventional subregioning scheme with the BEM to avoid dealing with the

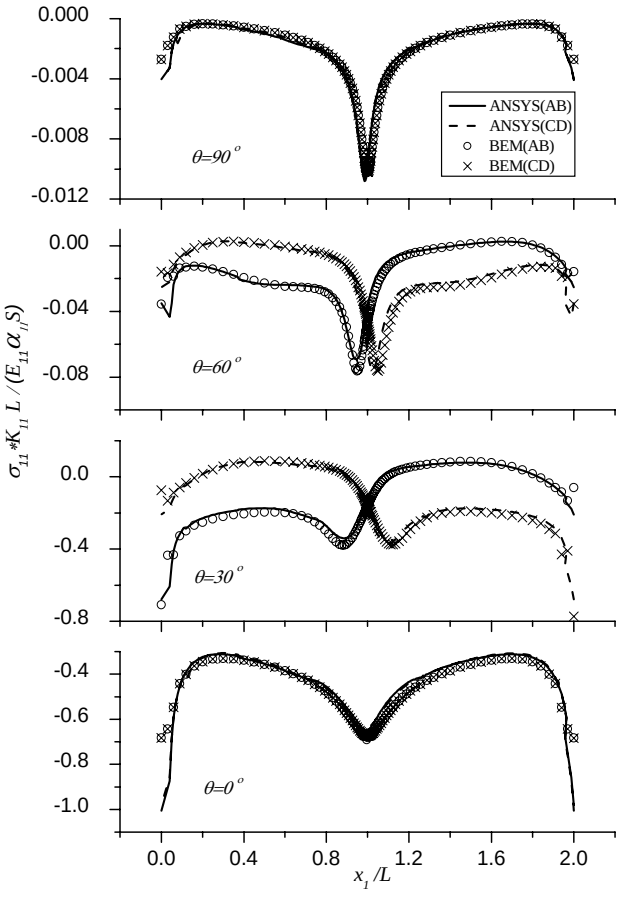

Figure 10 : Distribution of the normalized stress, $\sigma_{11}K_{11}L/E_{11}\alpha_{11}S$,along the constrained surfaces – Example 2

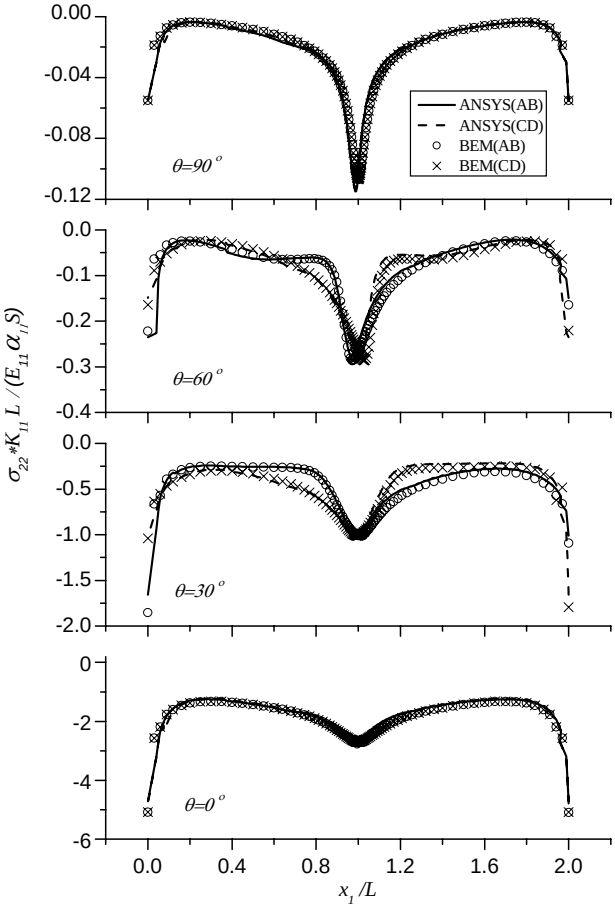

Figure 11 : Distribution of the normalized stress, $\sigma_{22}K_{11}L/E_{11}\alpha_{11}S$, along the constrained surfaces – Example 2

extra line integrals on the right-hand side of Eq. 47 when treating a multiply connected domain, as explained earlier. This was not followed, however, in order to demonstrate the generality of the formulation developed.

The boundary discretization of the BEM model in which 82 quadratic elements were employed, is also shown in Fig. 13. To investigate the effects of anisotropy, the problem was also solved for various rotation angles of the principal axes, namely, 0°, 30°, 60°, and 90°. Figure 14 shows the FEM mesh used with ANSYS, containing a total of 1558 (PLANE77 and PLANE82) elements. The variations of the computed normalized hoop stress around the circumference of the hole for the different orientation angles of the material principal axes are shown in Fig. 15. Similar results for the normalized direct stress components along the outer edges *AB*, *BC*, *DC*, and *AD* are shown in Fig. 16 to 19, respectively. From the comparison of the results shown in these figures, it can be seen that the BEM results are in very satisfactory agreement indeed with the corresponding FEM results obtained with ANSYS.

5 Conclusions

In this paper, the BEM has been developed for two dimensional thermoelastic stress analysis of an anisotropic medium with concentrated heat sources. This physical problem in anisotropic elasticity has many practical applications in engineering but its solution using the BEM remains extremely scarce indeed. The presence of concentrated heat sources gives rise to thermal singularities at their point locations that pose additional difficulties

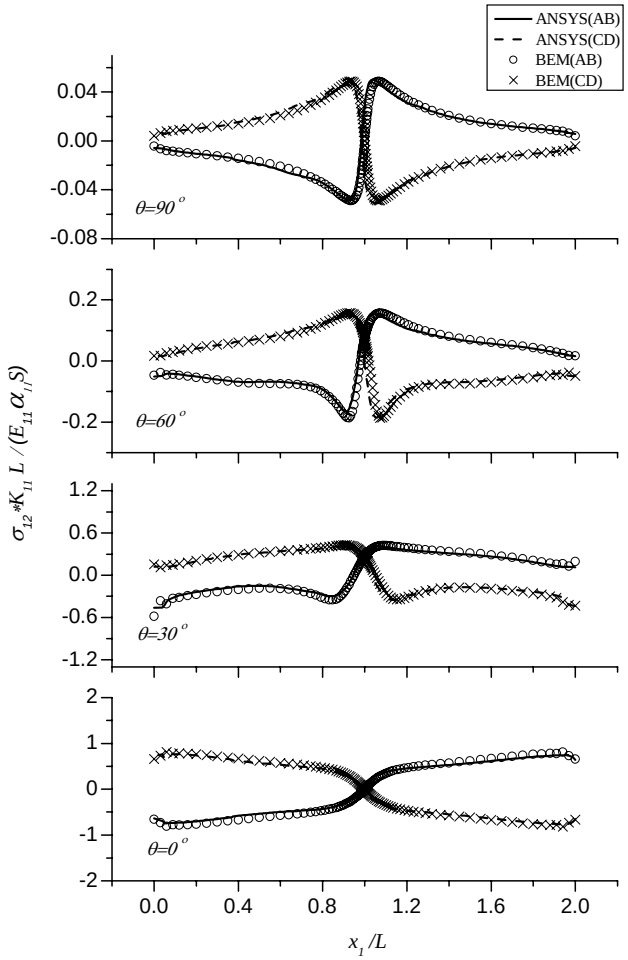

Figure 12 : Distribution of the normalized stress, $\sigma_{12}K_{11}L/E_{11}\alpha_{11}S$, along the constrained surfaces – Example 2

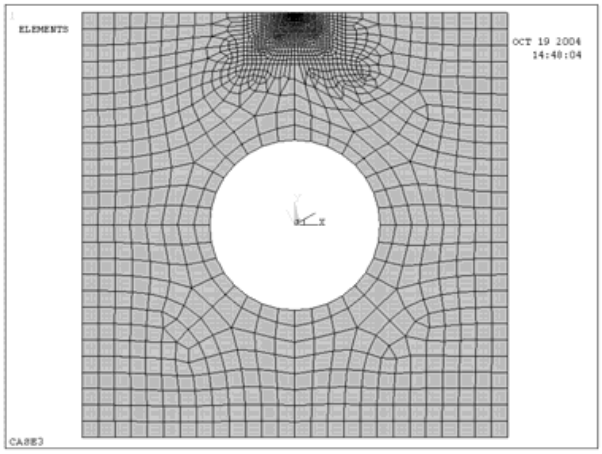

Figure 13 : A square plate with a central hole subjected to a point heat source on the boundary - Example 3

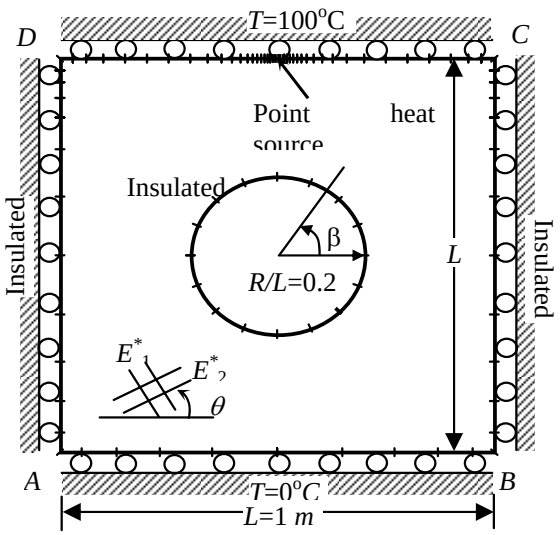

Figure 14 : FEM mesh for analysis with ANSYS – Example 3

in the derivation of the exact boundary integral equation (BIE). In the derivation of the BIE, the volume integral associated with the thermal loading needs to be transformed into boundary integrals. The exact transformation has been successfully achieved by a direct domain mapping technique in which the singularity is analytically removed in the mapped plane; the steps for which have been elucidated in the paper. Three example problems have been provided to demonstrate the veracity of the analytical and numerical formulations of the BEM. Their numerical results have been compared with those obtained using the FEM with the commercial code ANSYS, and excellent agreement between them have been obtained. The work has also provided illustrations of the ease with which the problems can be modeled using the BEM.

Acknowledgement: The first two authors gratefully acknowledge the financial support by the National Science Council of Taiwan, Republic of China (Grant Number: NSC-93-2212-E-035-006) and the Feng Chia University Distinguished Research Program (Grant Number: FCU-93GB15).

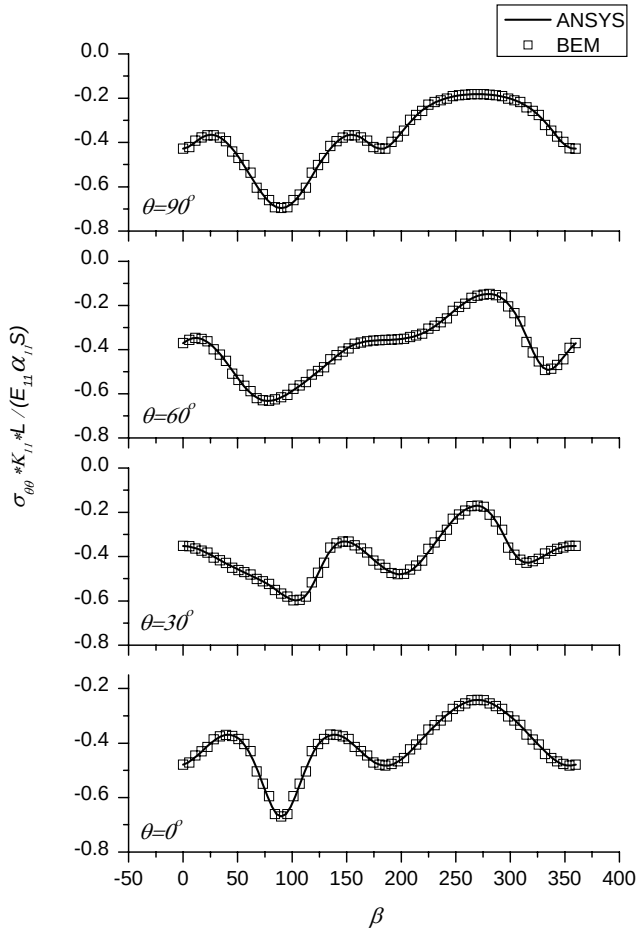

Figure 15 : Distribution of the hoop stress around the circumference of the hole – Example 3

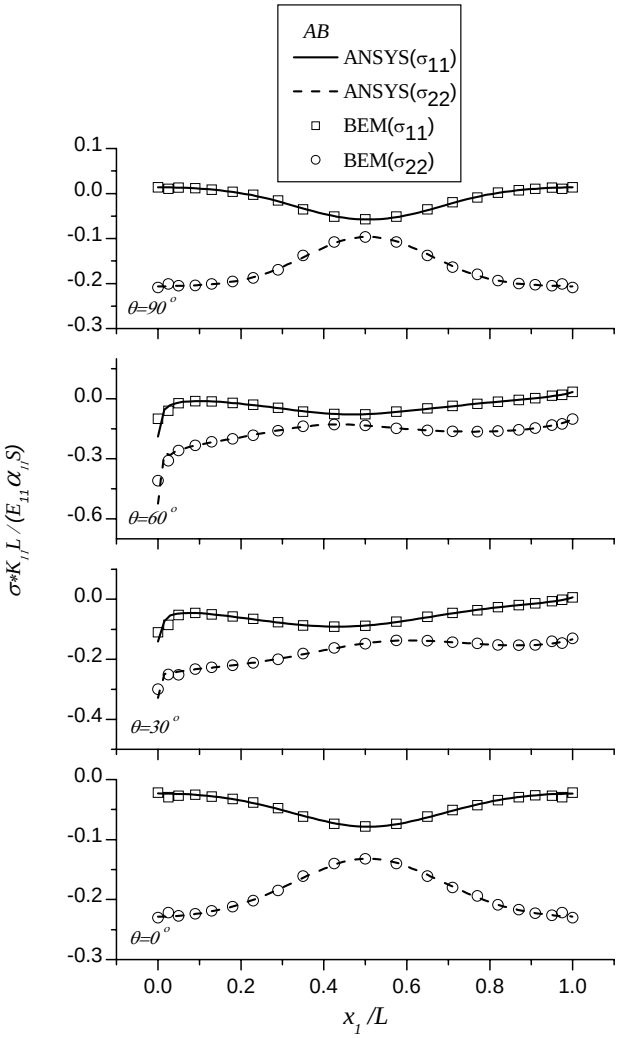

Figure 16 : Distributions of the direct stresses along the side *AB* – Example 3

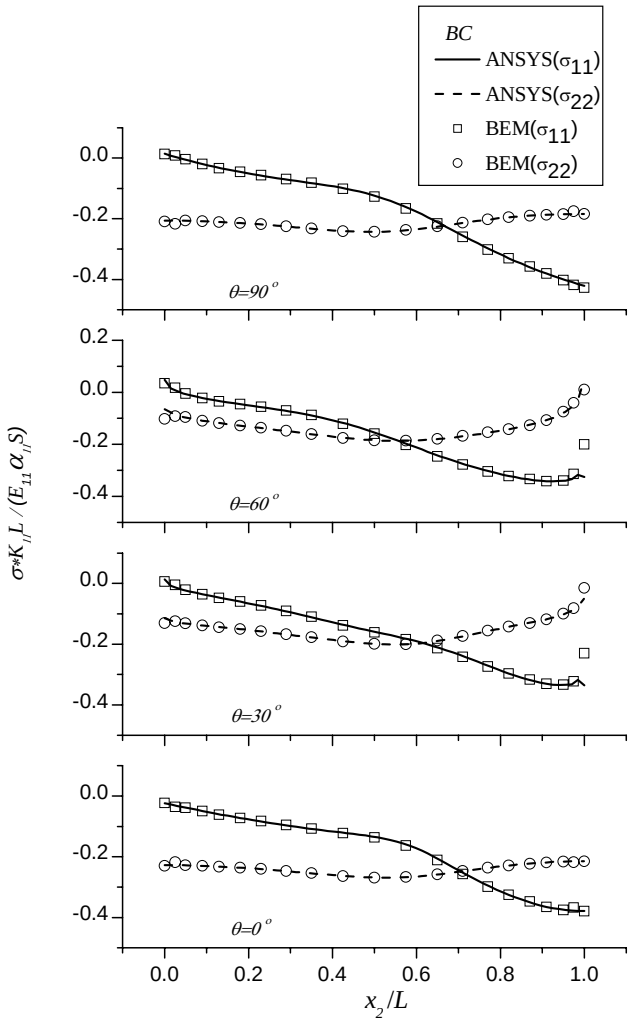

Figure 17 : Distributions of the direct stresses along the side *BC* – Example 3

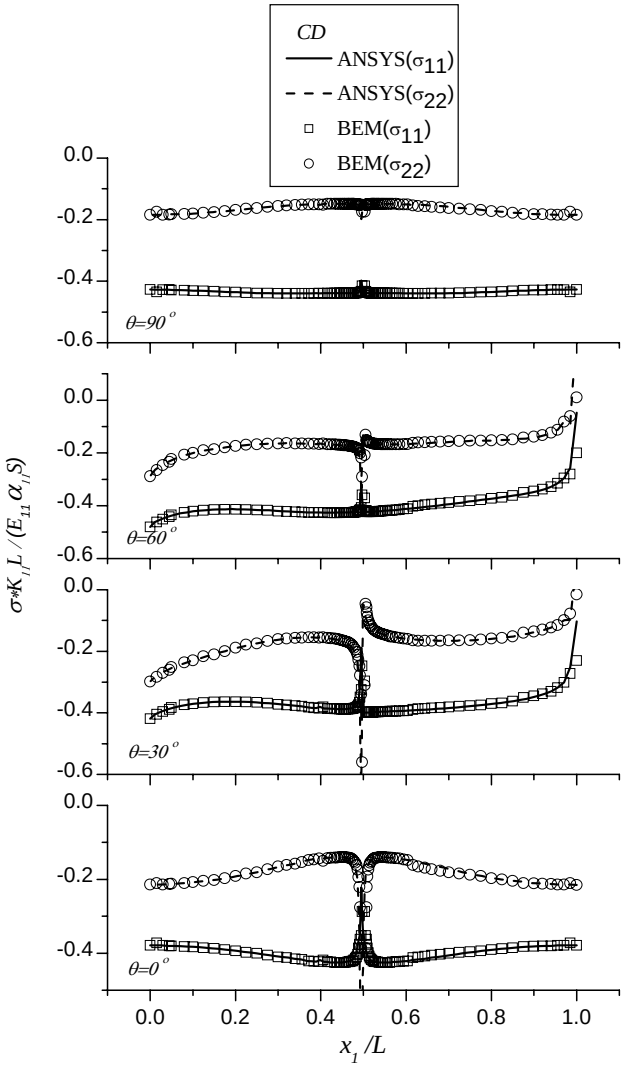

Figure 18 : Distributions of the direct stresses along the side *CD* – Example 3

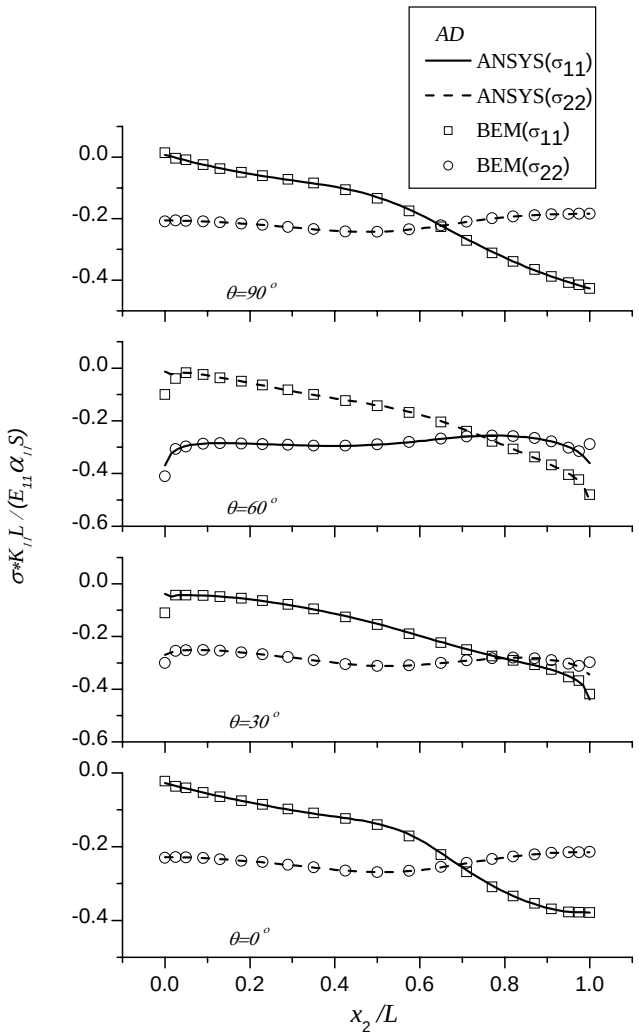

Figure 19 : Distributions of the direct stresses along the side *AD* – Example 3

References

Banerjee, P. K.; Butterfield, R. (1981): *Boundary Element Methods in Engineering Science*, McGraw-Hill, Maidenhead.

Bruch, E.; Lejeune, A. (1989): An effective solution of the numerical problems at multi-domain points for anisotropic Laplace problems, In *Advances in Boundary Elements* Vol. 2, Proc. 11^{th} Int. Conf. Boundary Element Methods, Cambridge, MA, USA, C.A. Brebbia and J.J. Connor (Eds.), Spring-Verlag, Berlin, pp. 3-14.

Camp, C. V.; Gipson, G. S. (1992): *Boundary Element Analysis of Nonhomogeneous Biharmonic Phenomena,* Springer-Verlag, Berlin.

Cheng, A. H. D.; Chen, C. S.; Golberg, M. A.; Rashed, Y. F. (2001): BEM for thermoelasticity and elasticity with body forces – a revisit, *Engng. Analysis Boundary Elements*, Vol. 25, pp. 377-387.

Clements, D. L. (1973): Thermal stress in an anisotropic elastic half-space, *SIAM J. Appl. Math.*, Vol. 24, pp. 332-337.

Deb, A.; Banerjee, P. K. (1990): BEM for general anisotropic 2D elasticity using particular integrals, *Commun. Appl. Num. Mech.*, Vol. 6, pp. 111-119.

Li, W. H. (1983): *Fluid Mechanics in Water Resources Engineering*, Allyn and Bacon, Toronto.

Mera, N. S.; Elliott, L.; Ingham, D. B.; Lesnic, D. (2001): A comparison of boundary element method formulations for steady state anisotropic heat conduction problems, *Engng. Analysis Boundary Elements*, Vol. 25, pp. 115-128.

Nardini, D.; Brebbia C. A. (1982): A new approach to free vibration analysis using boundary elements. In: *Boundary Element Methods in Engineering*, Computational Mechanics Publications, Southampton, pp. 312-326.

Nowak, A. J.; Brebbia, C. A. (1989): The multiple reciprocity method: A new approach for transforming BEM domain integrals to thebBoundary. *Engng. Analysis Boundary Elements,* Vol. 6, pp. 164-167.

Ochiai, Y.; Sladek, V. (2004): Numerical treatment of domain integrals without internal cells in three-dimensional BIEM formulations, *CMES: Computer Modeling in Engineering & Sciences*, Vol. 6, pp. 525-536.

Oin, O-H. (1999): Thermoelectroelastic Green's function for thermal load inside or on the boundary of an elliptic inclusion, *Mech. Materials*, Vol. 31, pp. 611-626.

Rahman, M. (2003): The axisymmetric contact problem of thermoelasticity in the presence of an internal heat source, *Int. J. Engng. Sc.*, Vol. 41, pp. 1899-1911.

Rashed, Y. F. (2004): Green's first identity method for boundary-only solution of self-weight in BEM formulation for thick slabs, *CMC: Computers, Materials & Continua*, Vol 1, pp. 319-326.

Rizzo, F. L.; Shippy, D. J. (1977): An advanced boundary integral equation method for three-dimensional thermoelasticity. *Int. J. Numerical Methods Engng.*, Vol. 11,

pp. 1753-1768.

Segerlind, L. J. (1984): *Applied Finite Element Analysis*, John Wiley, New York.

Sherief, H. H.; Magahed, F. F. (1999): A two-dimensional thermoelasticity problem for a half space subjected to heat sources, *Int. J. Solids Struct.*, Vol. 36, pp. 1369-1382.

Shiah, Y. C.; Tan, C. L.(1997): BEM treatment of two-dimensional anisotropic field problems by direct domain mapping, *Engng. Analysis Boundary Elements*, Vol. 20, pp. 347-351.

Shiah, Y. C.; Tan, C. L. (1998): BEM Treatment of Two-Dimensional Anisotropic Field Problems by Direct Domain Mapping, *Engng. Analysis Boundary Elements*, Vol. 20, pp. 347-351.

Shiah, Y. C.; Tan, C. L. (1999a): Exact boundary integral transformation of the thermoelastic domain integral in BEM for general 2D anisotropic elasticity, *Computational Mech.*, Vol. 23, pp. 87-96.

Shiah, Y. C.; Tan, C. L. (1999b): Determination of interior point stresses in two-dimensional BEM thermoelastic analysis of anisotropic bodies, *Int. J. Solids Struct.*, Vol. 37, pp. 809-829.

Sladek, J.; Sladek, V.; Atluri, S. N. (2004): Meshless local Petrov-Galerkin method for heat conduction problem in an anisotropic medium, *CMES: Computer Modeling in Engineering & Sciences*, Vol. 6, pp. 309-318.

Zhang, J. J.; Tan, C. L.; Afagh, F. F. (1996a): An argument redefinition procedure in the BEM for 2D anisotropic elastostatics with body forces. In: *Proc. Symp. Mech. in Design*, Toronto, May 6-9, Meguid, S. A. (Ed), Vol. 1, pp. 349-358.

Zhang, J. J.; Tan, C. L.; Afagh, F. F. (1996b): A general exact transformation of body-force volume integral in BEM for 2D anisotropic elasticity. *Computational Mech.,* Vol. 19, pp. 1-10.